

Use of femtosecond laser-induced breakdown spectroscopy (fs-LIBS) for micro-crack analysis on the surface

W. Wessel^{a,*}, A. Brueckner-Foit^a, J. Mildner^b, L. Englert^b, L. Haag^b, A. Horn^b, M. Wollenhaupt^b, T. Baumert^b

^a Institute for Materials Engineering, University of Kassel, Moenchebergstrasse 3, 34109 Kassel, Germany

^b Institute of Physics and CINSaT, University of Kassel, Heinrich-Plett-Str. 40, 34132 Kassel, Germany

ARTICLE INFO

Article history:

Received 23 December 2009

Received in revised form 10 March 2010

Accepted 12 March 2010

Available online 16 March 2010

Keywords:

Short crack

Laser-induced breakdown spectroscopy

Fatigue crack growth

TiAl

Intermetallics

ABSTRACT

It is well-known that the initiation and propagation behaviour of small cracks is strongly influenced by the microstructure. In addition to the visible structure on the surface, in-depth information is essential for the evaluation of influencing factors. Investigations on micro-crack behaviour have been performed with intermetallic γ -based TiAl. Starter notches facilitate systematic studies as cracks initiate from notch tips. In this case artificial notches in the scale less than colony dimensions were prepared by femtosecond pulsed laser radiation, which causes no significant damage. After multistage tensile compression tests under increasing load, several small cracks were generated and analyzed in the SEM. Using femtosecond laser-induced breakdown spectroscopy (fs-LIBS) it was possible to analyze spectrochemically the surrounding microstructure of these micro-cracks and their propagation on the surface.

© 2010 Elsevier Ltd. All rights reserved.

1. Introduction

The fatigue damage accumulation of metal-based materials can be divided in to three parts. At first micro-structurally short cracks are initiated due to micro-plasticity. These cracks extend until they reach the size of the so-called physically small cracks. Both stages of crack growth are strongly influenced by the microstructure. The final stage of the fatigue damage accumulation process comes about when the worst crack starts to extend towards its critical size. In this stage the time to failure can be described by linear elastic fracture mechanics (LEFM) [1]. In many cases micro-crack initiation and propagation take up most of the lifetime. Consequently, the damage mechanisms in this regime have to be well understood for safe component design. A systematic study of small crack extension is rather time-consuming due to the numerous influencing factors which govern the crack initiation stage. Hence it is quite hard to get well-defined starting cracks. An alternative may be to use artificial micro-notches, e.g. made using the focus ion beam (FIB) technique. Another approach with more rapid machining rate is given by femtosecond pulsed laser radiation. It was shown [2,3] that micro-cracks are initiated from these artificial notches under cyclic loading. Using the fs-laser it has to be made sure that the heat affected zone formed by heat diffusion during processing is negligible and that the cracks initiated from these micro-notches possess extension mechanisms similar to those of natural small cracks [2].

Small cracks can propagate both intergranularly or transgranularly. A mixture of both extension modes can be observed in engineering materials with complex microstructure [4], where sometimes a transgranular crack path is observed on the

* Corresponding author. Tel.: +49 (0)561 804 3656; fax: +49 (0)561 804 3650.

E-mail address: w.wessel@uni-kassel.de (W. Wessel).

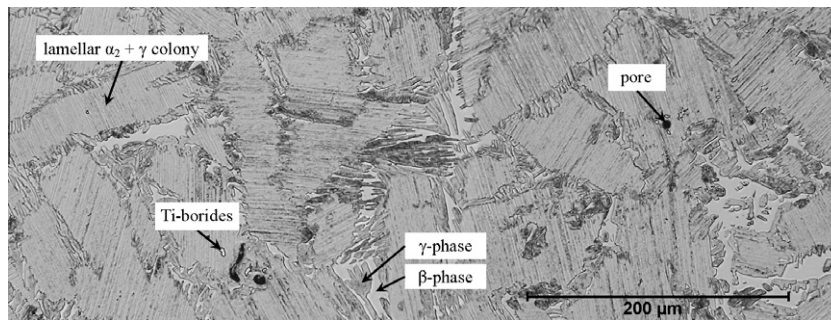


Fig. 1. Optical image of microstructure of the Ti-43Al-4Nb-1Mo-0.1B alloy.

surface and the same crack extends along phase boundaries in an intergranular mode or vice versa. Therefore a three-dimensional analysis of the crack path is crucial in understanding micro-crack growth. New insights in this problem may be gained by using the fs-laser again. Laser-induced breakdown spectroscopy (LIBS) combined with femtosecond laser radiation offers spectrochemical element analysis with a high spatial resolution in the range of μm [5]. Ablation of the material surrounding a crack on the sample surface using fs-LIBS can provide a useful tool for examining three-dimensional crack propagation in dependence of the local microstructure.

2. Material

Investigations of paths of micro-cracks were performed with an intermetallic γ -TiAl alloy. Because of its good specific properties up to 700 °C this material class is a promising candidate for structural components of turbines and combustion engines. Conventional γ -TiAl alloys consist primarily of colonies with lamellar arranged hard α_2 -phase (Ti_3Al , hexagonal DO_{19} structure) and relatively soft γ -phase (TiAl, tetragonal L1_0 structure). Optional heat treatment causes segregation of globular γ -grains and leads to a duplex or near lamellar microstructure.

There are numerous studies on the influence of microstructure on crack initiation and crack growth in lamellar titanium aluminides. The experiments show [6–10] that micro-cracks are initiated within the colonies in directions parallel to the lamellae. The angle between the initiation plane and the loading direction is either around $90 \pm 15^\circ$ or $45 \pm 15^\circ$. This is in agreement to the planes of maximum tensile and shear stresses, respectively, on lamellar interfaces, where the cohesive force is expected to be low. In the ensuing extension phase the crack may propagate in a translamellar or an interlamellar way or it can extend along colony boundaries. In all cases Mode-I is the most likely crack propagation mode. Cracks can be retarded if they have to cross lamellae as more energy is needed for the transgranular crack extension mode than for the intergranular one. A crack can be stopped, if it encounters lamellae with an orientation which strongly deviates from the crack plane.

In this study the relatively new texture-free β -solidifying cast TNM alloy with the following chemical composition Ti-43Al-4Nb-1Mo-0.1B (at.%) was used. Fig. 1 represents the etched microstructure of this alloy. Lamellar colonies have the size of 50–500 μm and typical lamellae thicknesses up to 2 μm . Distinctive colony boundaries comprise globular γ -grains and the third β -phase (bcc solid solution or B2 ordered variant). Existing porosity and Ti-boride segregations are a consequence of casting without Hot Isostatic Pressing (HIP) and the presence of Boron, respectively.

3. Femtosecond pulsed laser technique

The femtosecond laser system consists of a Ti:Sapphire fs-oscillator (Femtosource Scientific Pro, Femtolasers) and a Chirped-Pulse Multipass Amplifier (Femtopower Pro, Femtolasers). Pulses of 500 mW with a duration of 35 fs and a wavelength of 800 nm are generated at a repetition rate of 1 kHz. Single-shot control of the laser system enables different operation modes, i.e. single-shot, multi-shot and kHz mode. The laser radiation is guided to a modified microscope using a mirror system. A coupling mirror within the tube of the microscope allows changing between observation mode (for specimen positioning and observation) and fs-pulse mode. The positioning accuracy of the system is 10 nm. Fig. 2 gives an overview of the experimental setup.

In the experiments femtosecond pulses are focused through a microscope objective (50 \times , N.A. 0.5) onto the sample. As the energy of the laser pulse exceeds the threshold for material ablation, a plasma is created on the specimen surface. The emitted plasma luminescence is collimated and guided into a spectrometer by an optical fibre. A gated intensified CCD camera is used to record the emission spectrum of each single laser pulse. Analysis of the characteristic lines emitted by the plasma enables the detection of specific elements in the material. Additionally the intensity of these emission lines can be related to the number of atoms of the element in the plasma and is a convenient way to determine the local chemical composition of the material in question and therefore its microstructure.

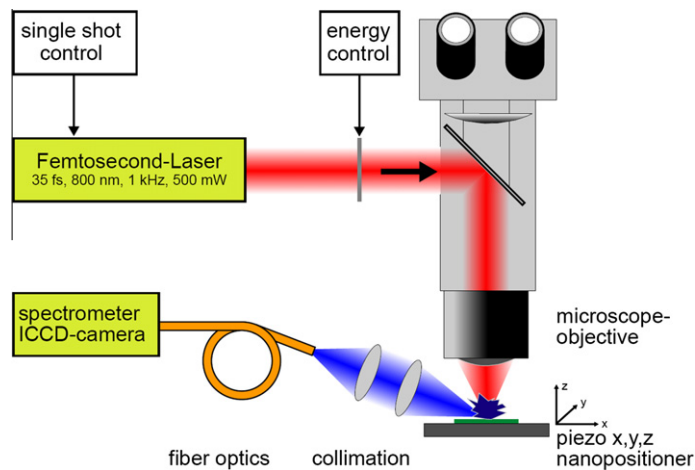


Fig. 2. Schematic illustration of experimental setup.

Another application of fs-LIBS in materials engineering is the analysis of crack paths in the early stages of crack initiation or growth. The signal is reduced significantly when crossing a crack as the ablated volume of the material is diminished. Both aspects of fs-LIBS are used in the following to study the extension of small cracks in a TiAl-intermetallic alloy.

4. Experiments

4.1. Analysis of material phases with energy dispersive X-ray technique

Energy dispersive X-ray technique (EDX) was used in order to obtain reference values for the phase composition. The results are summarised in Table 1. It should be noted that analysis of γ - and α_2 -phases were done on wide lamellae. However the values can be somewhat uncertain as Monte Carlo simulations of electron interaction in such phases show that the interaction volume can exceed the lamellae size. Nevertheless EDX measurement results from the literature [11–14] on similar alloys possessing globular microstructure are comparable to present ones. Much more precise measurements with three dimensional atomic probe (3DAP) microscopy on lamellae [15] show slight differences in the chemical composition of α_2 -phase with a ratio of 59.20:32.41 at.% (Ti:Al).

4.2. Micro-crack initiation

Micro-cracks were initiated in smooth specimens under stepwise increasing loading and under fatigue loading. The first test was performed by using a smooth flat specimen with an hourglass shape. The load train started with a tension–compression load cycle with a small load leading to a stress level of 50 MPa in the smallest cross section of the specimen. The maximum load was increased in steps in the following cycles. First deviations from linear elastic behaviour were detected at a stress level of 400 MPa. The first micro-cracks were observed at the load level of 625 MPa. The specimen fractured at a maximum load of 655 MPa with a fracture strain of 0.56%. The small value of the fracture strain indicates that the material is relatively brittle and that a small increase of the load may lead to catastrophic failure by unstable extension of a micro-crack. After fracture several micro-cracks were detected in the vicinity of the fatal crack which were analysed in more detail using fs-LIBS.

The second test was a regular load-controlled push–pull fatigue test ($R = -1$) with a cylindrical specimen. Smooth notches were introduced on two sides which allowed to observe the specimen surface during the test with the help of a travelling long-distance optical microscope. Fracture occurred after 151,062 load cycles at a load level of 400 MPa, corresponding to the

Table 1

EDX results of chemical composition of major phases (at.%).

Phase/segregation	Ti	Al	Nb	Mo
γ	51.13	43.51	4.28	1.08
α_2	55.91	38.95	4.18	0.96
β /B2	57.09	34.68	5.20	3.04
Ti-boride*	83.43	1.59	12.76	2.22

* Boron is not listed because of its low atomic weight and consequently high measurement errors.

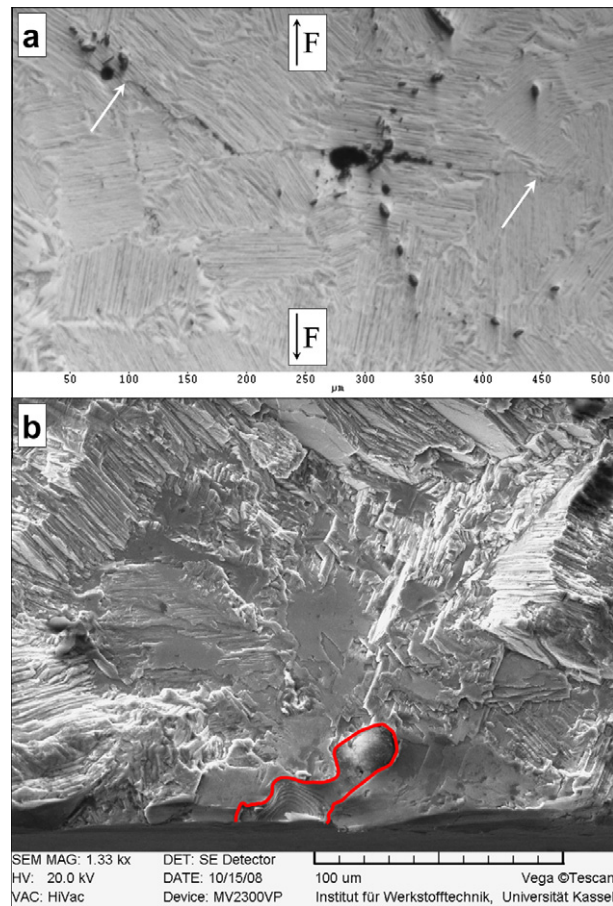


Fig. 3. Crack initiation and propagation in TiAl-alloy depending on microstructure: ((a) optical image after 150,000 load cycles and (b) SEM micrograph of fracture surface with the pore).

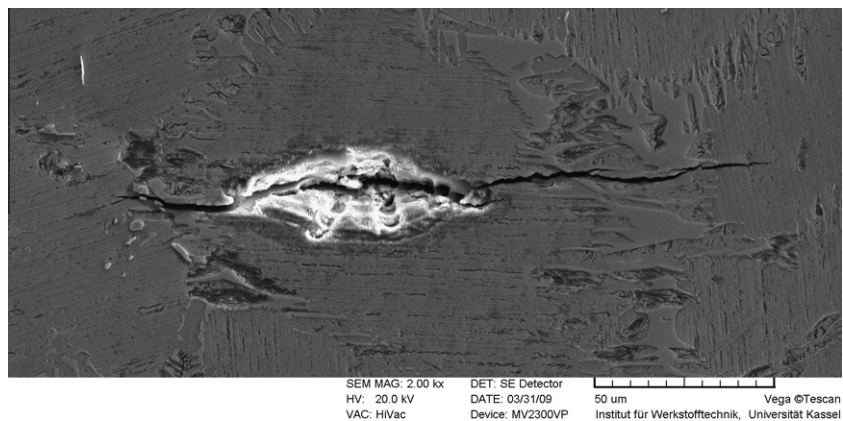


Fig. 4. Micro-crack initiation from an artificial notch.

onset of plastic deformation in the afore mentioned quasi-static tests. Fig. 3 shows how the fatal crack was first initiated from a large pore, then had a certain amount of microstructure controlled growth and reached a size just below its critical size after 150,000 load cycles. A detailed analysis of the pore after the fracture showed that it had a maximum diameter of about $32\ \mu\text{m}$ at the surface and $65\ \mu\text{m}$ in depth direction.

A third test was performed using artificial notches introduced at well-defined locations in the microstructure, see Fig. 4. The size of these notches was defined on the basis of the results of the second test, as the artificial notches have to be larger

than the fatal natural flaws for obvious reasons. The sizes of the notch were 70 μm length, 20 μm width, and about 20 μm depth, with the depth depending on the parameters of the laser system. The load level was selected to be just below the plastic limit (375 MPa). The lifetime of the specimen amounted to 435,835 load cycles until final fracture. However, the crack shown in Fig. 4 was not the fatal one, but was initiated just before failure occurred. The fatal crack started from the backside of the specimen.

4.3. Laser-induced breakdown spectroscopy of micro-cracks and phases

In order to develop the mapping technique for micro-crack analysis by femtosecond laser-induced breakdown spectroscopy, the lateral resolution of fs-LIBS was determined in the first step. For this purpose SEM micrographs of surface modifications induced by fs-material processing at different laser fluences were investigated. In these SEM micrographs different morphologies are apparent in the single- and multi-shot mode (Fig. 5a left and right, respectively). These morphologies are due to different processes induced by fs-laser radiation in the focal point on the sample surface (Fig. 5b). Depending on the local intensity these processes are: heterogeneous melting, homogeneous melting, vaporisation and phase explosion (see Fig. 5).

At laser fluences below the threshold for material ablation, two regions can be detected in the SEM corresponding to two different melt dynamics. The lighter region on the outside (within the dashed line in Fig. 5a left) is attributed to resolidified melt induced by heterogeneous thermal melting already taking place at very small laser fluences below the threshold for material ablation. The ring structure (dotted line) is attributed to homogeneous non-thermal melting, i.e. ultrafast melting, due to a larger intensity in the central region of femtosecond laser excitation still below the threshold for ablation [16]. The diameter of the ring structure relates to the threshold fluence for ultrafast melting. The droplet formation of the ring is due to the surface tension present during resolidification [17]. The thickness of these melting layers is associated to the optical absorption length of the metal at the applied laser wavelength being in the range of tens of nanometers [18]. Therefore the material modifications in this area are negligible. As soon as the laser fluence exceeds the threshold for material ablation, further structures are visible. At medium fluences a smooth ablation structure is created with an outer diameter referred to D_{out} , representing the region of melt ejection. In this regime normal vaporisation takes place [19], in which the melt phase is laterally displaced due to the recoil of the expanding vapour [20]. At higher fluences the ablation crater itself becomes visible due to phase explosion of the now superheated melting layer [19]. The inner diameter D_{in} is detected gradually in the SEM micrographs for increasing laser fluence. Applying several laser pulses at the same spot of the sample, the characteristics discussed above are more distinct even at small and medium laser fluences due to accumulation effects [19,21]. The outer diameter D_{out} is larger than the inner diameter D_{in} for increasing pulse energy (Fig. 6). As the chemical sampling at one ablation spot is of main interest, the outer diameter represents the relevant quantity for the mapping technique describing the strongly influenced area during laser ablation (determined via SEM analysis).

For fs-LIBS the signal strength of the plasma luminescence is of central interest. In order to be able to analyze the spectrochemical information during the fs-LIBS mapping, a sufficient signal of the plasma luminescence is required. Fig. 7 shows the line signal of TiAl at 395 nm as well as the continuum signal at line position against the pulse energy for both single- and multi-shot mode. Spectra are described in more detail below (see also Fig. 8).

With increasing pulse energy, the line signal for a single-shot can be detected distinctly from the corresponding continuum signal at 200 nJ. In this pulse energy regime the outer diameter of the ablation structures has increased significantly. However at small diameters, i.e. small pulse energies, no significant line signal is detected. In order to overcome this problem, multi-shot irradiation is used (10 shots per position), whereas the spectra were accumulated on the ICCD-chip. At 20 nJ pulse energy a poor line to continuum signal ratio is achieved. Additionally the outer diameter is about 50% larger compared

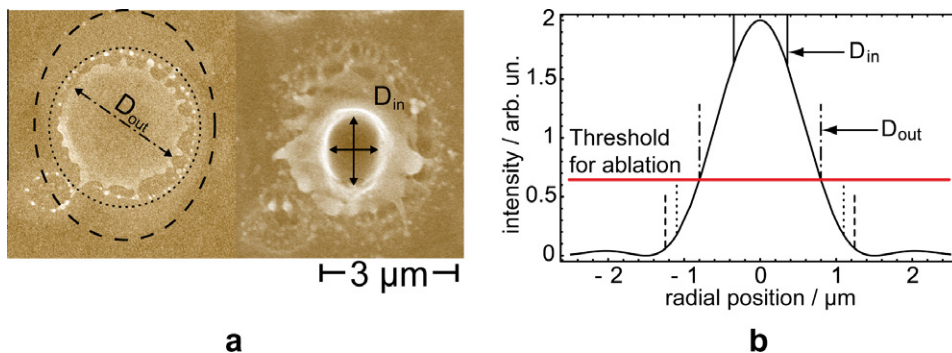


Fig. 5. (a) SEM micrographs of ablation structures at 100 nJ pulse energy (left: single-shot; right: 10 shots) and (b) calculated radial intensity distribution in the focal point on the sample surface (for a N.A. 0.5 objective). Dashed line: threshold for heterogeneous melting; dotted line: threshold for homogeneous melting; dash-dotted line: Threshold for vaporisation; solid line: threshold for phase explosion.

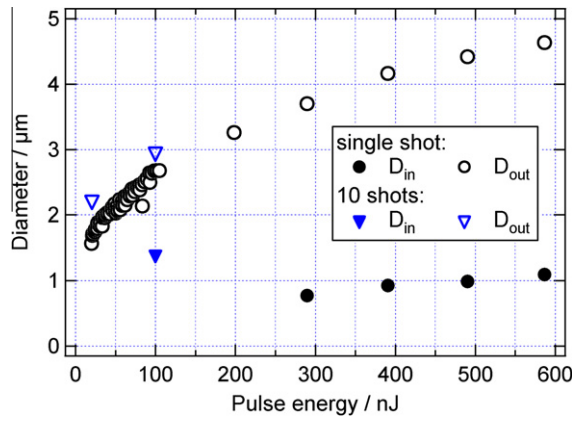


Fig. 6. Inner and outer diameter versus pulse energy at single-shot and multi-shot mode.

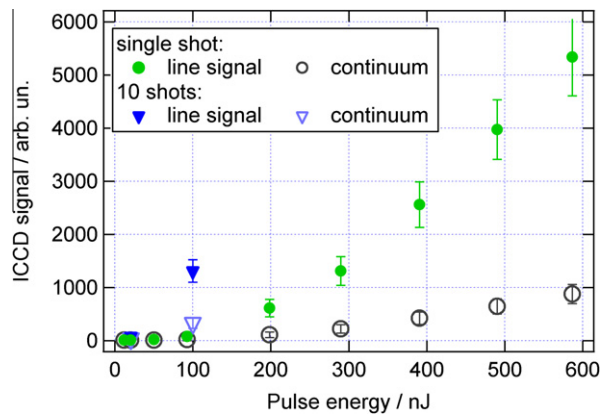


Fig. 7. Line signal of TiAl at 395 nm and continuum signal at line position versus pulse energy at single- and multi-shot mode.

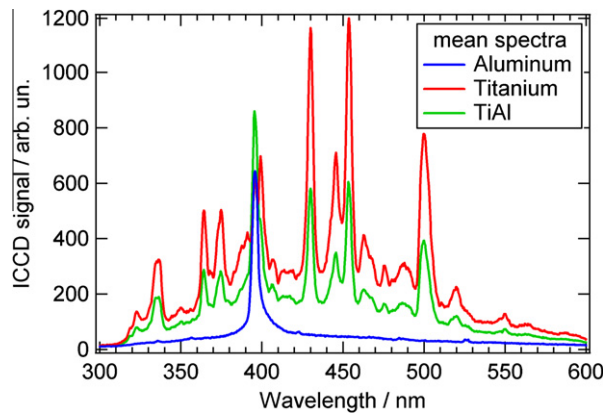


Fig. 8. Averaged emission spectra of pure aluminium (99.9%), pure titanium (Grade 2) and TiAl.

to the single-shot diameter. In the case of 100 nJ pulse energy the line signal is distinctly detectable from the continuum signal. This could be attributed to an increased ablation efficiency [22]. The corresponding outer diameter only increases by 15% compared to single-shot irradiation. As a compromise between sufficient LIBS signals and a high spatial resolution, respectively, a pulse energy of 100 nJ with 10 laser shots per position is chosen.

As is mentioned above, the chemical sampling at an individual ablation spot is of main interest for this scanning mapping technique. Therefore an optimal lateral step size between the individual ablation spots is crucial. This means a compromise has to be found between a maximal spatial resolution (small step size with overlapping ablation craters) and a minimally influenced region of the adjacent ablation structures (no overlapping). To determine this parameter, several two-dimensional fs-LIBS scans have been performed each with different distances between the ablation spots. Down to a step size of 2 μm , the LIBS signal is constant and decreases below this value. This is consistent with the detected inner diameter of 1.6 μm of the ablation structures. By choosing a step size of 2 μm the regions of melt ejection (D_{out}) are slightly overlapping, but there is no overlap of the ablation craters (D_{in}) (Fig. 6). Note that for three-dimensional mapping an approach with uniform material removal has also advantages. In summary the following parameters for two-dimensional fs-LIBS mapping were chosen: a pulse energy of 100 nJ (corresponding to an intensity of $1.9 \times 10^{14} \text{ W/cm}^2$ and a fluence of 6.5 J/cm^2), 10 shots per position and a lateral step size of 2 μm .

For spectrochemically resolved fs-LIBS mapping, the characteristic emission spectra of the sample system (i.e. the characteristic emission spectra of all constituents) in the observed spectral region have to be known. The detected emission spectra of aluminium, titanium and TiAl show characteristic lines and continuum emission as displayed in Fig. 8. These averaged spectra were taken for pure aluminium (99.9%) and titanium (Grade 2) samples, which were polished before irradiation.

The emission spectrum of aluminium features two lines at 394 and 396 nm, which are not resolved separately by the spectrometer used in this experiment. The emission spectrum of titanium consists of many lines being in good accordance with data from NIST spectroscopic database. Both titanium and TiAl emission spectra have been measured for different pulse energies (100–1000 nJ) ensuring that the ratio between the maximal line signals is constant. Furthermore, the linear combination of the reference spectra matches the TiAl spectrum for the same pulse energies very well. This calibration set has been used in order to extract qualitatively the fraction of aluminium and titanium at every measurement point (details will be given in the following).

5. Results

During the fatigue test, a micro-crack was initiated from the notch in Fig. 4, which first propagated in an interlamellar mode. This is also true for the propagation in depth direction. After crossing the intercolonial phase it continues in a pure mode-I propagation mode. Crack growth was retarded due to the fact that both crack tips encountered unfavourably oriented lamellae after a certain amount of crack extension. That is why final fracture was caused by a crack emanating from a large subsurface pore on the backside of the specimen. Further investigations of micro-crack initiation from the micro-notches are under way.

With the mapping parameters determined in Section 4.3, a two-dimensional scan of a TiAl surface with simultaneous detection of the fs-LIBS signal was performed. The investigated TiAl sample (TNM, see Section 2) exhibits very small micro-cracks which were initiated by microindentation points used for geometric calibration (Fig. 9a). The micro-crack on the left-hand side has a width of about 2.2 μm , the one on the right-hand side about 1.2 μm at indicated positions in Fig. 9a.

During the fs-LIBS scan, one accumulated spectrum (consisting of 10 single-shot spectra) is detected at each single ablation spot. After subtraction of a constant background each spectrum has been integrated over the spectral region shown in Fig. 8. The signal strength at each point is plotted in a two-dimensional graph, i.e. a fs-LIBS map, in Fig. 9b. The dominating feature is the microindentation. As both micro-cracks are clearly detectable, a μm -resolution of this two-dimensional fs-LIBS mapping technique is achieved. An enlargement of the detected micro-crack on the left-hand side is shown in Fig. 9c for further inspection. Furthermore a SEM micrograph of the sample surface after fs-LIBS is shown in Fig. 9d with an enlarged view of the ablation structures (inset) demonstrating the spatially separated laser-induced structures.

The fs-LIBS data of the surface scan in Fig. 9 were analyzed as is described in Section 4.3, getting a spectrochemically resolved mapping of the sample surface and the micro-cracks at the same time. Fig. 10 shows fs-LIBS maps in which the titanium fraction (a) and the aluminium fraction (b) of the investigated sample surface are plotted, respectively.

In Fig. 10a again both the microindentation and the micro-cracks are clearly visible. The two lamellar phases (see Fig. 1 in Section 2) cannot be detected by fs-LIBS as their lateral dimensions are below the spatial resolution of this actual setup. Therefore the LIBS signal in this area (i.e. ablation volume) is a mixture of both phases resulting in averaged titanium and aluminium fraction values. The lighter regions indicated in Fig. 9a correspond to the colony boundary (β -phase) which consists of a higher titanium fraction compared to the mixture of the lamellar phases as seen in the EDX measurements (Table 1). This can also be seen from the anticorrelation between Fig. 10a and b within the highlighted areas. As the TNM alloy consists mainly of titanium and aluminium, a rise in titanium fraction corresponds to a drop in aluminium fraction and vice versa.

A preliminary crack path analysis using fs-LIBS was performed on the secondary cracks found in the first test. A SEM micrograph of this crack is displayed in Fig. 11a. The fs-LIBS scan was performed with the mapping parameters mentioned in Section 4.3. The normalized titanium signal (Fig. 11b) qualitatively shows an increase in the area of the colony boundary (β -phase) which corresponds to EDX measurements (Table 1). The more uniform signal on the left-hand side of the micro-crack is due to a difference in height of the sample surface after fracture. The lower level with respect to the laser focus position results in an overall decreased LIBS signal.

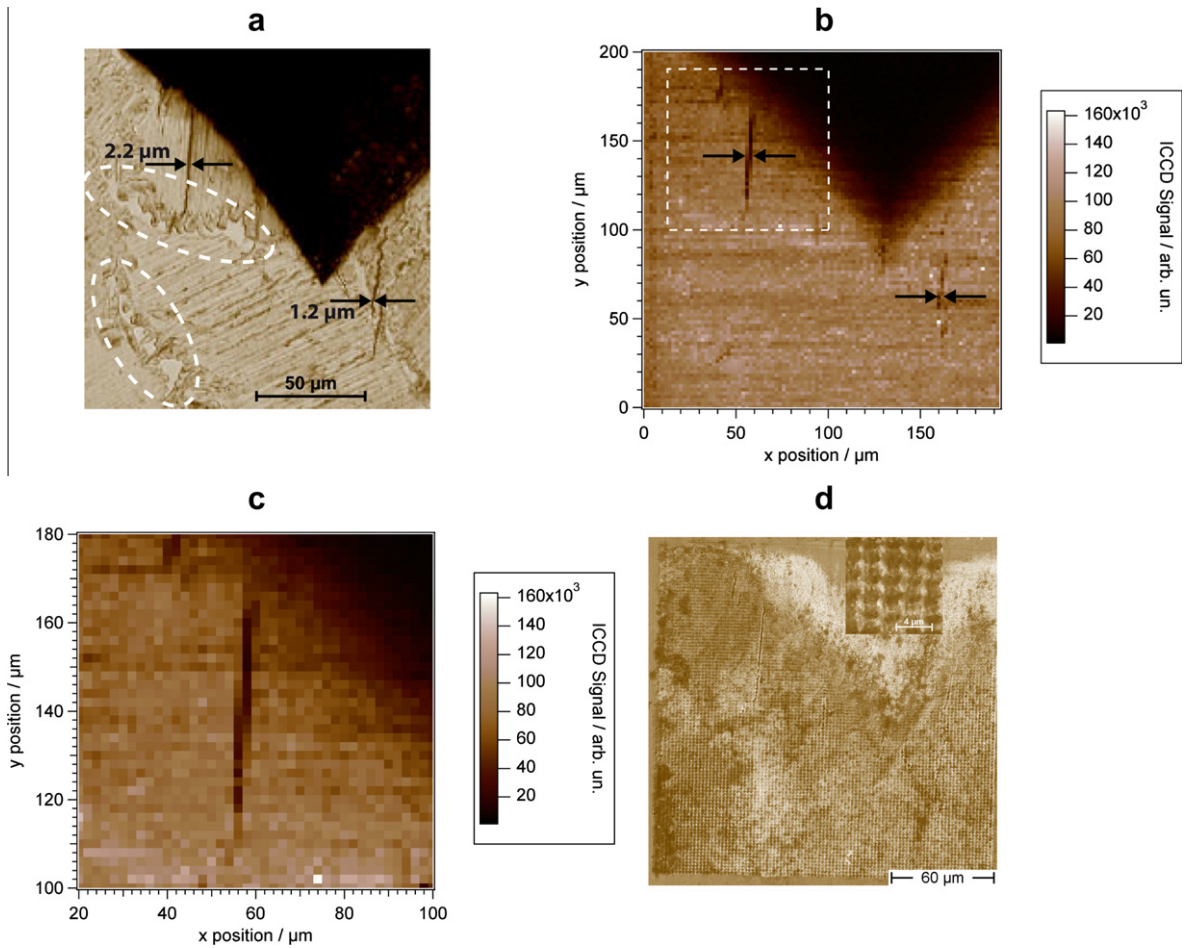


Fig. 9. (a) Optical image of sample surface before ablation, (b) fs-LIBS map, (c) enlargement of fs-LIBS map at micro-crack position, and (d) SEM micrograph after fs-LIBS scan.

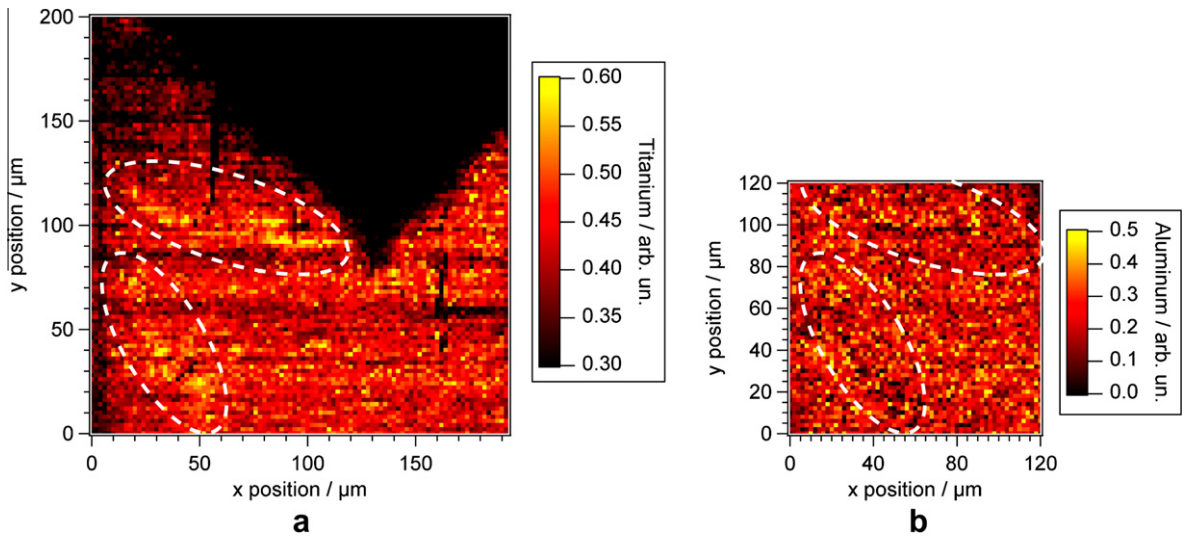


Fig. 10. fs-LIBS maps of the same sample surface as in Fig. 9a: ((a) titanium fraction and (b) aluminium fraction in a smaller area of interest).

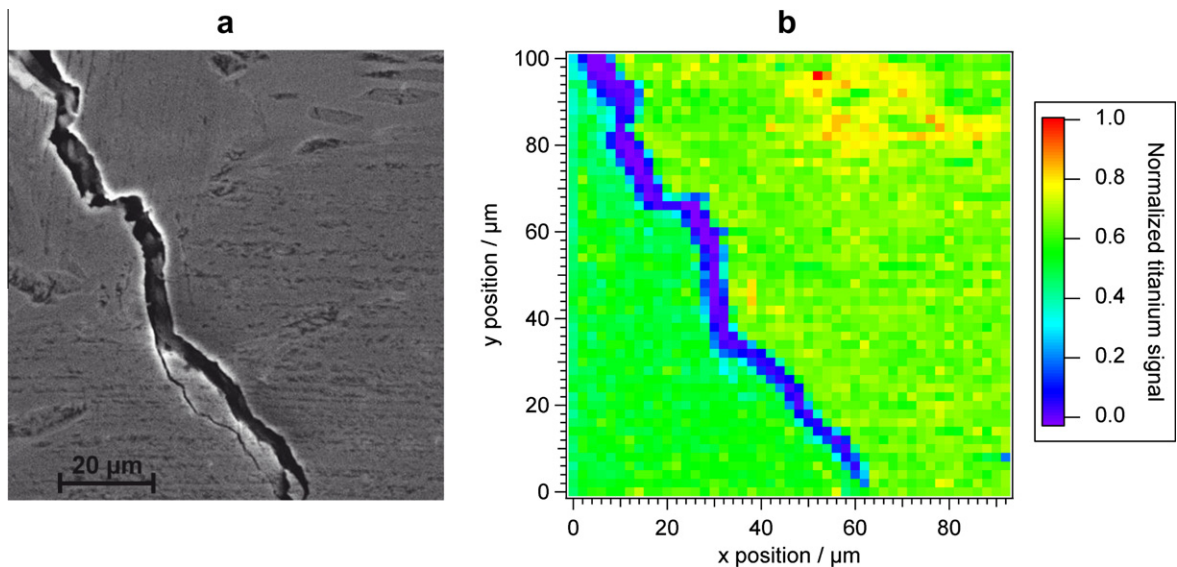


Fig. 11. (a) SEM micrograph of sample surface before ablation and (b) fs-LIBS map.

6. Conclusion

By combining fs-LIBS with a scanning microscope, a setup was developed which possesses spectrochemical sensitivity with spatial resolution in the μm range, and allows crack reconstruction on the μm scale. In this work a lateral step size of $2 \mu\text{m}$ was demonstrated.

Future work will concentrate on further developing this technique for three-dimensional crack reconstruction and three-dimensional spectrochemical analysis. In order to increase the spatial resolution, current research is focused on investigating to what extent temporal structured pulses on the femtosecond and picosecond time scale increase the spectrochemical sensitivity. A similar idea was used in micromachining of dielectrics where asymmetric pulses led to structures one order of magnitude below the diffraction limit [23,24].

Three-dimensional crack reconstruction together with spectrochemical sensitivity on the μm scale will help to understand the extension mechanisms of small cracks and their interaction with microstructure.

Acknowledgements

The authors thank the German Science Foundation DFG for financial support and GfE Gesellschaft für Elektrometallurgie mbH for providing the test material.

References

- [1] Anderson TL. Fracture mechanics: fundamentals and applications. Boca Raton: Taylor & Francis Group; 2005.
- [2] Motoyashiki Y, Brückner-Foit A, Englert L, Haag L, Wollenhaupt M, Baumert T. Use of femtosecond laser technique for studying physically small cracks. *Int J Fract* 2006;139:561–8.
- [3] Shyam A, Allison JE, Jones JW. A small fatigue crack growth relationship and its application to cast aluminum. *Acta Mater* 2005;53:1499–509.
- [4] Motoyashiki Y, Brückner-Foit A, Sugeta A. Investigation of small crack behaviour under cyclic loading in a dual phase steel with an FIB tomography technique. *Fatigue Fract Eng Mater Struct* 2007;30:556–64.
- [5] Assion A, Wollenhaupt M, Haag L, Mayorov F, Sarpe-Tudoran C, Winter M, Kutschera U, Baumert T. Femtosecond laser-induced breakdown spectrometry for Ca^{2+} analysis of biological samples with high spatial resolution. *Appl Phys, B* 2003;77:391–7.
- [6] Kruzic JJ, Campbell JP, Ritchie RO. On the fatigue behavior of γ -based titanium aluminides: role of small cracks. *Acta Mater* 1999;47:801–16.
- [7] Hamada S, Hamada H, Suzuki H, Tamin MN, Nozue A. Microstructure and environment-dependent fatigue crack propagation properties of Ti-48Al intermetallics. *J Mater Sci* 2002;37:1107–13.
- [8] Cao R, Zhu H, Chen JH, Zhang J, Yao HJ. Effects of microcrack-damage on fracture behavior of TiAl alloy part I displacement-controlled tensile test. *Mater Sci Eng A* 2008;474:1–14.
- [9] Arata JJM, Kumar KS, Curtin WA, Needleman A. Crack growth in lamellar titanium aluminide. *Int J Fract* 2001;111:163–89.
- [10] Evangelista E, Zhang WJ, Francesconi L, Nazmy M. Toughening mechanism in the lamellar and duplex TiAl-based alloys at ambient temperature: microcrack analysis. *Scripta Metall Mater* 1995;33:467–72.
- [11] Chen, S. (1988). Microstructural analyses of intermetallic TiAl(Nb)-compounds prepared by arc melting and by powder metallurgy. PhD thesis. Germany: GKSS-Forschungszentrum Geesthacht GmbH.
- [12] Sun F-S, Cao C-X, Kim S-E, Lee Y-T, Yan M-G. Alloying mechanism of beta stabilizers in a TiAl alloy. *Metall Mater Trans A* 2001;32A:1573–89.
- [13] Hamzah E, Kanniah M, Harun M. Effect of chromium addition on microstructure, tensile properties and creep resistance of as-cast Ti-48Al alloy. *J Mater Sci* 2007;42:9063–9.

- [14] Imayev V, Imayev R, Khismatullin T, Güther V, Beck W, Fecht H-J. Superplastic behavior of Ti–43Al–7(Nb,Mo)–0.2B alloy in the cast + heat-treated condition. *Scripta Mater* 2007;57:193–6.
- [15] Gerstl SSA, Kim Y-W, Seidman DN. Atomic scale chemistry of α_2/γ interfaces in a multi-component TiAl alloy. *Interface Sci* 2004;12:303–10.
- [16] Sokolowski-Tinten K, Bialkowski J, Boing M, Cavalleri A, von der Linde D. Thermal and nonthermal melting of gallium arsenide after femtosecond laser excitation. *Phys Rev B* 1998;58:805–8.
- [17] Kim J, Na S. Metal thin film ablation with femtosecond pulsed laser. *Opt Laser Technol* 2007;39:1443–8.
- [18] Ma S, McDonald JP, Tryon B, Yalisove SM, Pollock TM. Femtosecond laser ablation regimes in a single-crystal superalloy. *Metall Mater Trans A* 2007;38A:2349–57.
- [19] Mannion PT, Magee J, Coyne E, O'Connor GM, Glynn TJ. The effect of damage accumulation behaviour on ablation thresholds and damage morphology in ultrafast laser micro-machining of common metals in air. *Appl Surf Sci* 2004;233:275–87.
- [20] Krüger J, Meja P, Autric M, Kautek W. Femtosecond pulse laser ablation of anodic oxide coatings on aluminum alloys on-line acoustic observation. *Appl Surf Sci* 2002;186:374–80.
- [21] Korte F, Adams S, Egbert A, Fallnich C, Ostendorf A, Nolte S, Will M, Ruske J-P, Chichkov BN, Tünnermann A. Sub-diffraction limited structuring of solid targets with femtosecond laser pulses. *Opt Expr* 2000;7:41–9.
- [22] Winefordner JD, Gornushkin IB, Correll T, Gibb E, Smith BW, Omenetto N. Comparing several atomic spectrometric methods to the super stars: Special emphasis on laser induced breakdown spectrometry, LIBS, a future super star. *J Anal At Spectrom* 2004;19:1061–83.
- [23] Englert L, Rethfeld B, Haag L, Wollenhaupt M, Sarpe-Tudoran C, Baumert T. Control of ionization processes in high band gap materials via tailored femtosecond pulses. *Opt Expr* 2007;15:17855–62.
- [24] Wollenhaupt M, Englert L, Horn A, Baumert T. Control of ionization processes in high band gap materials. *JLMN* 2009;4:144–51.